1

Urban Mapping Requirements

1.1 Introduction

Urban landscapes are typically a complex combination of buildings, roads, parking lots, sidewalks, garden, cemetery, soil, water, and so on. Each of the urban component surfaces possesses unique biophysical properties and relates to their surrounding environment to create the spatial complexity of urban ecological systems and landscape patterns. To understand the dynamics of patterns and processes and their interactions in heterogeneous landscapes such as urban areas, one must be able to quantify accurately the spatial pattern of the landscape and its temporal changes (Wu et al. 2000). In order to do so, it is necessary (i) to have a standardized method to define theses component surfaces and (ii) to detect and map them in repetitive and consistent ways, so that a global model of urban morphology may be developed, and monitoring and modeling their changes over time be possible (Ridd 1995).

Impervious surfaces are anthropogenic features through which water cannot infiltrate into the soil, such as roads, driveways, sidewalks, parking lots, rooftops, and so on. In the past two decades, impervious surface has emerged not only as an indicator of the degree of urbanization, but also a major indicator of environmental quality (Arnold and Gibbons 1996). Impervious surface is a unifying theme for all participants at all watershed scales, including planners, engineers, landscape architects, scientists, social scientists, local officials, and others (Schueler 1994). The magnitude, location, geometry, and spatial pattern of impervious surfaces, and the pervious–impervious ratio in a watershed have hydrological impacts. Although land-use zoning emphasizes roof-related impervious surfaces, transport-related impervious surfaces could have a greater impact. The increase of impervious cover would lead to the increase in the volume, duration, and intensity of urban runoff (Weng 2001), and an overall decrease of groundwater recharge and baseflow but an increase

Techniques and Methods in Urban Remote Sensing, First Edition. Qihao Weng.

Published 2020 by John Wiley & Sons, Inc.

of stormflow and flood frequency (Brun and Band 2000). Furthermore, imperviousness is related to the water quality of a drainage basin and it's receiving streams, lakes, and ponds (Hurd and Civco 2004). In addition, the areal extent and spatial occurrence of impervious surfaces may significantly influence urban climate by altering sensible and latent heat fluxes within the urban canopy and boundary layers (Yang et al. 2003). Therefore, estimating and mapping impervious surface is significant to a range of issues and themes in environmental science central to global environmental change and human–environment interactions and has been regarded as a key variable in urban remote sensing studies. The data sets of impervious surfaces are valuable not only for environmental management, e.g. water quality assessment and storm water taxation, but also for urban planning, e.g. building infrastructure and sustainable urban development.

Remote sensing technology has been widely applied in urban land-use and land-cover (LULC) classification and change detection. However, it is rare that the classification accuracy of greater than 80% can be achieved by using per-pixel classification (so-called "hard classification") algorithms (Mather 1999, p. 10). Therefore, the "soft"/fuzzy approach of LULC classifications has been applied, in which each pixel is assigned a class membership of each LULC type rather than a single label (Wang 1990). Nevertheless, as Mather (1999) suggested, either "hard" or "soft" classifications was not an appropriate tool for the analysis of heterogeneous landscapes. Mather (1999) maintained that identification/description/quantification, rather than classification, should be applied in order to provide a better understanding of the compositions and processes of heterogeneous landscapes such as urban areas. Ridd (1995) proposed a major conceptual model for remote sensing analysis of urban landscapes, i.e. the vegetation–impervious surface–soil (V-I-S) model. It assumes that land cover in urban environments is a linear combination of three components, namely, vegetation, impervious surface, and soil. Ridd believed that this model can be applied to spatial-temporal analyses of urban morphology, biophysical, and human systems. Having realized that the V-I-S model may be used as a method to define standardized urban landscape components, this chapter employs linear spectral mixture analysis (LSMA) as a remote sensing technique to estimate and map V-I-S components in order to analyze urban pattern and dynamics. The case study will be conducted in Indianapolis, United States, from 1991 to 2000, by using multi-temporal satellite images, i.e. Landsat Thematic Mapper (TM)/Enhanced Thematic Mapper Plus (ETM+) imagery of 1991, 1995, and 2000. Because of the significance of impervious surface as an urban land cover, land use, or material, this chapter will start with examining data requirements for remote sensing of impervious surfaces, with a particular interest in the impacts of remotely sensed data characteristics (i.e. spectral, temporal, and spatial resolutions).

1.2 Spectral Resolution Requirement

Remote sensing of impervious surfaces should consider the requirements for mapping three interrelated entities or substances on the Earth surface (i.e. material, land cover, and land use) and their relationships. Mapping of each entity/substance must consider the spectral resolution of a remote sensor. The spectral features include the number, locations, and bandwidths of spectral bands. The number of spectral bands can range from a limited number of multispectral bands (e.g. 4 bands in SPOT data and 7 for Landsat TM) to a medium number of multispectral bands (e.g. Advanced Spaceborne Thermal Emission and Reflection Radiometer [ASTER] with 14 bands and Moderate Resolution Imaging Spectroradiometer [MODIS] with 36 bands) and to hyperspectral data (e.g. AVIRIS and EO-1 Hyperion images with 224 bands). A large number of spectral bands provide the potential to derive detailed information on the nature and properties of different surface materials on the ground, but it also means a difficulty in image processing and a large data redundancy due to high correlation among the adjacent bands. Increase of spectral bands may improve classification accuracy, only when those bands are useful in discriminating the classes (Thenkabail et al. 2004a).

Urban areas are composed of a variety of materials, including different types of artificial materials (i.e. impervious surfaces), soils, rocks and minerals, and green and non-photosynthetic vegetation. These materials comprise land cover and are used in different manners for various purposes by human beings. Land cover can be defined as the biophysical state of the earth's surface and immediate subsurface, including biota, soil, topography, surface and ground water, and human structures (Turner et al. 1995). Land use can be defined as the human use of the land and involves both the manner in which the biophysical attributes of the land are manipulated and the purpose for which the land is used (Turner et al. 1995). Remote sensing technology has often been applied to map land use or land cover, instead of materials. Each type of land cover may possess unique surface properties (material), however, mapping land covers and materials have different requirements (Figure 1.1). Land-cover mapping needs to consider characteristics in addition to those coming from the material (Herold et al. 2006). The surface structure (roughness) may influence the spectral response as much as the intra-class variability (Gong and Howarth 1990; Myint 2001; Shaban and Dikshit 2001; Herold et al. 2006). Two different land covers, for example, asphalt roads and composite shingle/tar roofs, may have very similar materials (hydrocarbons) and thus are difficult to discern, although from a material perspective, these surfaces can be mapped accurately with hyperspectral remote sensing techniques (Herold et al. 2006). Therefore, land-cover mapping requires taking into account of the intra-class variability and spectral separability. On the other hand, analysis of land-use classes would nearly be impossible with spectral information alone.

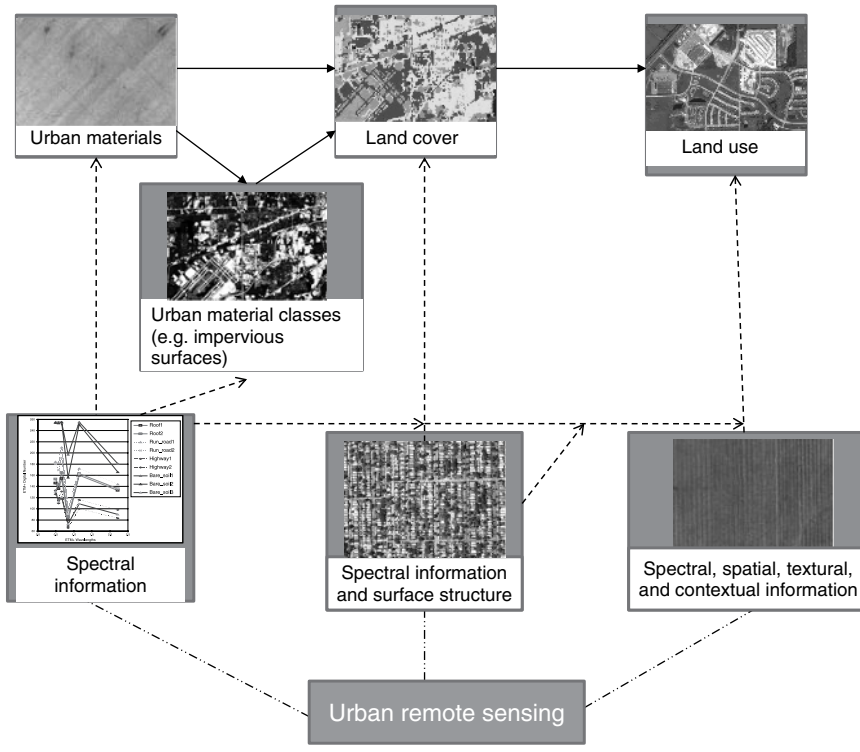

Figure 1.1 Illustration of the relationship among remote sensing of urban materials, land cover, and land use. *Source:* after Weng and Lu (2009). Reproduced with permission of Taylor & Francis.

Additional information, such as spatial, textural, and contextual information, is usually required in order to have a successful land-use classification in urban areas (Gong and Howarth 1992; Stuckens et al. 2000; Herold et al. 2003).

LSMA has been widely used in impervious surface estimation, implying that impervious surface is a type of surface material. This view has much to do with the spectral resolution of a remote sensor. LSMA is a physically deterministic modeling method that decomposes the signal measured at a given pixel into its component parts called end-members (Adams et al. 1986; Boardman 1993; Boardman et al. 1995). End-members are regarded as recognizable surface materials that have homogenous spectral properties all over the image. Impervious surfaces can be extracted and mapped as a single end-member or the combination of two or more end-members (Rashed et al. 2003; Wu and Murray 2003; Lu and Weng 2006a; Weng et al. 2008, 2009). Previous research has largely applied LSMA to medium spatial resolution, multispectral images, such as Landsat TM/ETM+ and Terra's ASTER images, for extraction

of impervious surfaces (Weng 2007). However, both spatial and spectral resolution is regarded as too coarse for use in urban environments because of the heterogeneity and complexity of urban impervious surface materials. In the LSMA model, the maximum number of end-members is directly proportional to the number of spectral bands used. Hyperspectral imagery may be more effective in extracting end-members than multispectral imagery. The vastly increased dimensionality of a hyperspectral sensor may remove the sensor-related limit on the number of end-members available. More significantly, the fact that the number of hyperspectral image channels far exceeds the likely number of end-members for most applications readily permits the exclusion from the analysis of any bands with low signal-to-noise ratios or with significant atmospheric absorption effects (Lillesand et al. 2004). In previous research, hyperspectral data have been successfully used for land-use/cover classification (Benediktsson et al. 1995; Hoffbeck and Landgrebe 1996; Platt and Goetz 2004; Thenkabail et al. 2004a, 2004b), vegetation mapping (McGwire et al. 2000; Schmidt et al. 2004; Pu et al. 2008), and water mapping (Bagheri and Yu 2008; Moses et al. 2009). As spaceborne hyperspectral data such as EO-1 Hyperion become available, research and applications with hyperspectral data will increase. Weng et al. (2008) found a Hyperion image was more powerful in discerning low-albedo surface materials, which has been a major obstacle for impervious surface estimation with medium-resolution multispectral images. A sensitivity analysis suggested that the improvement of mapping accuracy in general and the better ability in discriminating low-albedo surfaces resulted largely from additional bands in the mid-infrared region (Weng et al. 2008).

The spectral characteristics of land surfaces are the fundamental principles for land imaging. Previous studies have examined the spectral properties of urban materials (Hepner et al. 1998; Ben-Dor et al. 2001; Herold et al. 2003; Heiden et al. 2007) and spectral resolution requirements for separating them (Jensen and Cowen 1999). When Jensen and Cowen (1999) explained minimum spectral resolution requirements for urban mapping, the discussion focused mainly on multispectral imagery data. They suggested that spatial resolution was more important than spectral resolution in urban mapping. The spectrum from visible to near infrared (NIR), mid-infrared (MIR), and microwave are suitable for LULC classification at coarser categorical resolutions (e.g. Levels I and II of the Anderson classification); however, at the finer categorical resolutions (e.g. Levels III and IV of the Anderson classification) and for extraction of buildings and roads, panchromatic band is needed (Jensen and Cowen 1999). Other urban studies had employed hyperspectral sensing for discriminating among urban surface features based on their diagnostic absorption and reflection characteristics and for detailed identification of urban materials. Hepner et al. (1998) suggested that interferometric synthetic aperture radar (IFSAR) imagery, when combined with AVIRIS data, can provide information on 3D geometry, topography, and impervious surfaces,

and other urban surface characteristics. Ben-Dor et al. (2001) examined the feasibility of using detailed spectral information in the spectral region of 0.4–1.1 μm for identifying different features in the urban environment using Compact Airborne Spectral Imager (CASI) data. Herold et al. (2003) found that several bands in the visible, NIR, and SWIR regions were best suited for distinguishing different urban features and emphasized that both reflection and absorption features due to material composition in the SWIR region was significant in urban land-cover classification, especially in separating different types of impervious surfaces. Heiden et al. (2007) presented a hierarchical classification method for the derivation of diagnostic urban spectral features that can be used for an automated identification of spectrally homogeneous end-members from hyperspectral image data.

1.3 Temporal Resolution Requirement

Temporal resolution refers to the amount of time it takes for a sensor to return to a previously imaged location, commonly known as the repeat cycle or the time interval between acquisitions of two successive images. For airborne remote sensing, temporal resolution is less pertinent, since users can schedule flights for themselves. Jensen and Cowen (1999) suggested that studies of urban development, buildings and property infrastructure, and road center lines only need to have an image every one to five years. They further suggested that the temporal resolution requirement should be a bit higher for delineating precise road width, namely, one to two years. However, Herold (2007) believed that road aging and deterioration may have various temporal resolution depending upon the quality of pavement, traffic, and distresses (e.g. cracks, raveling, etc.).

Temporal differences between remotely sensed imageries are not only caused by the changes in spectral properties of the Earth's surface features/objects, but they can also result from atmospheric differences and changes in sun position during the course of a day and during the year. Temporal resolution is a very important consideration in remote sensing of vegetation, because vegetation grows according to daily, seasonal, and annual phenological cycles. Weng et al. (2009) found that a summer ASTER image was better for estimation of impervious surfaces than a spring (April) and a fall (October) one; based on a case study in Indianapolis, USA, it is suggested that mapping of impervious surfaces tended to be more accurate with contrasting spectral response from green vegetation (GV) when LSMA technique was employed. Plant phenology caused changes in the variance partitioning and impacted the mixing space characterization, leading to a less accurate estimation of impervious surfaces in the spring and fall (Weng et al. 2009). When other methods are used, detection of urban buildings and roads may well be suited in the leaf-off season in the temperate regions. In addition, the set overpass times of satellites may

coincide with clouds or poor weather conditions. This is especially true in the tropical and coastal areas, where persistent clouds and rains in the wet season offer limit clear views of the Earth's surface and thus prevent from getting good quality images (Lu et al. 2008). In consideration of the impact of street trees on impervious surfaces, Linden and Hostert (2009) suggested that the quantification of this impact was generally possible by performing multi-temporal analyses at leaf-on/leaf-off seasons, but solar illumination geometry and shadowing can presumably preclude leaf-off acquisitions for many temperate cities.

The off-nadir imaging capability of satellite sensors, such as SPOT-5, IKONOS, and Quickbird, reduces the usual revisit time depending on the latitude of the imaged areas. This feature is designed for taking stereoscopic images and for producing digital elevation models, but it obviously also allows for more frequent coverage of selected regions for short periods and provides another means for monitoring and assessing impervious surfaces.

1.4 Spatial Resolution Requirement

Spatial resolution is a function of sensor altitude, detector size, focal size, and system configuration (Jensen 2005). It defines the level of spatial detail depicted in an image, and it is often related to the size of the smallest possible feature that can be detected from an image. This definition implies that only objects larger than the spatial resolution of a sensor can be picked out from an image. However, a smaller feature may sometimes be detectable if its reflectance dominates within a particular resolution cell or it has a unique shape (e.g. linear features). Another meaning of spatial resolution is that a ground feature should be distinguishable as a separate entity in the image. But the separation from neighbors or background is not always sufficient to identify the object. Therefore, the concept of spatial resolution includes both detectability and separability. For any feature to be resolvable in an image, it involves consideration of spatial resolution, spectral contrast, and feature shape. Jensen and Cowen (1999) suggested that the minimum spatial resolution requirement should be one-half the diameter of the smallest object of interest. For two major types of impervious surface, buildings (perimeter, area, height, and property line) and roads (width) are generally detectable with the minimum spatial resolution of 0.25–0.5 m, while road centerline can be detected at a lower resolution of 1–30 m (Jensen and Cowen 1999). Before 1999, lack of high spatial resolution (less than 10 m) images is a main reason for scarce research in remote sensing of impervious surfaces before 2000. Cracknell (1999) asserted that NOAA's AVHRR had been the major instrument for remote sensing studies between 1980 and 1999, and that Landsat or SPOT was not mentioned among the 12 most cited papers published in the International Journal of Remote Sensing during this period. The medium (10–100 m) spatial resolution images, such as

Landsat and SPOT, were not readily available and were expensive. Many researchers employed per-pixel classifiers and applied successful experience in vegetation mapping to remote sensing of impervious surfaces (Gillies et al. 2003; Carlson 2004; Bauer et al. 2007). This approach can avoid a major problem that existed in the medium-resolution imagery, i.e. mixed pixels.

Mixed pixels dominate in coarse resolution images such as AVHRR and MODIS. However, for a remote sensing project, image spatial resolution is not the only factor needed to consider. The relationship between the geographical scale of a study area and the spatial resolution of remote sensing image has to be studied (Quattrochi and Goodchild 1997). For mapping at the continental or global scale, coarse spatial resolution data are usually employed. Gamba and Herold (2009) assessed eight major research efforts in global urban extent mapping and found that most maps were produced at the spatial resolution of 1–2 km. When using coarse resolution images, a threshold has to be defined with respect to what constitute a built-up/impervious pixel (Lu et al. 2008; Schneider et al. 2010). Reliable impervious surface data that derive from medium-resolution imagery are helpful for validating and predicting urban/built-up extent at the coarse resolution level (Lu et al. 2008).

With the advent of very high-resolution satellite imagery, such as IKONOS (launched 1999), QuickBird (2001), and OrbView (2003) images, great efforts have been made in the applications of these remote sensing images in urban and environmental studies. High-resolution satellite imageries have been applied in impervious surface mapping (Cablk and Minor 2003; Goetz et al. 2003; Lu and Weng 2009; Wu 2009; Hu and Weng 2011). These fine spatial resolution images contain rich spatial information, providing a greater potential to extract much more detailed thematic information (e.g. land use and land cover), cartographic features (buildings and roads), and metric information with stereo-images (e.g. height and area). These information and cartographic characteristics are highly beneficial to estimating and mapping of impervious surfaces. The proportion of mixed pixels is significantly reduced in an image scene. However, some new problems come with these image data, notably shadows caused by topography, tall buildings, or trees (Dare 2005), and the high spectral variation within the same land-cover class (Hsieh et al. 2001). Shadows obscure impervious surfaces underneath and thus increase the difficulty to extract both thematic and cartographic information. These disadvantages may lower image classification accuracy if classifiers used cannot effectively handle them (Irons et al. 1985; Cushnie 1987). In order to make full use of the rich spatial information inherent in fine spatial resolution data, it is necessary to minimize the negative impact of high intra-spectral variation. Algorithms that use the combined spectral and spatial information may be especially effective for impervious surface extraction in the urban areas (Lu and Weng 2007).

1.5 Linear Spectral Mixture Analysis of Urban Landscape

The prevalence of mixed pixels in urban areas implies that the instantaneous field of the view of the medium-resolution sensors does not match with the operational scale of the landscapes. Such landscapes are better viewed as a continuum formed by continuously varying proportions of idealized materials, just as soils may be described in terms of the proportions of sand, silt, and clay (Mather 1999). Agricultural land in the Midwest United States, residential areas, and semiarid areas are typical examples of continuum-type landscapes.

LSMA is a method that has been widely employed to handle the mixed pixel problem, besides the fuzzy classification. Instead of using statistical methods, LSMA is based on physically deterministic modeling to unmix the signal measured at a given pixel into its component parts called end-members (Adams et al. 1986; Boardman 1993, Boardman et al. 1995). End-members are recognizable surface materials that have homogenous spectral properties all over the image. LSMA assumes that the spectrum measured by a sensor is a linear combination of the spectra of all components within the pixel (Boardman 1993). Because of its effectiveness in handling spectral mixture problem and ability to provide continuum-based biophysical variables, LSMA has been widely used in (i) estimation of vegetation cover (Asner and Lobell 2000; McGwire et al. 2000; Small 2001; Weng et al. 2004; Lee and Lathrop 2005), (ii) impervious surface estimation and/or urban morphology analysis (Phinn et al. 2002; Wu and Murray 2003; Rashed et al. 2003; Lu and Weng 2006a, 2006b; Wu et al. 2005), (iii) vegetation or land-cover classification (Adams et al. 1995; Cochrane and Souza 1998; Aguiar et al. 1999; Lu and Weng 2004), and (iv) change detection (Rashed et al. 2005; Powell et al. 2007). However, with a few exceptions, these studies have focused on technical specifics and on the examination of the effectiveness of LSMA. Only a few studies have explicitly adopted the V-I-S model as the conceptual model to explain urban land-cover patterns (Phinn et al. 2002; Wu and Murray 2003; Wu et al. 2005; Lu and Weng 2006a, 2006b; Powell et al. 2007), while others implicitly (Rashed et al. 2003, 2005). Rashed et al. (2005) and Powell et al. (2007) are the only research attempts to examine urban land-cover "change" with the V-I-S model. Rashed et al. (2005) assessed changes between landscape components aggregated to census tracts in Cairo, Egypt, but determination of the thresholds of change may be problematic since they may vary from image to image. Powell et al. (2007) identified the stages of urban development by selecting four neighborhoods from an image of Manaus, Brazil, which did not involve change detection from multi-temporal satellite images. This chapter applies the V-I-S concept for a spatial-temporal analysis of the urban morphology in Indianapolis with LSMA, and by doing so, the potentials and limitations of

this model for characterizing and quantifying urban landscape components can further be examined.

The mathematical model of LSMA can be expressed as

$$R_i = \sum_{k=1}^{n} f_k R_{ik} + E_i \tag{1.1}$$

where $i = 1, \ldots, m$ (number of spectral bands); $k = 1, \ldots, n$ (number of end-members); R_i is the spectral reflectance of band i of a pixel which contains one or more end-members; f_k is the proportion of end-member k within the pixel; R_{ik} is the known spectral reflectance of end-member k within the pixel in band i; and E_i is the error for band i. To solve f_k, the following conditions must be satisfied: (i) selected end-members should be independent of each other, (ii) the number of end-members should not be larger than the spectral bands used, and (iii) selected spectral bands should not be highly correlated. A constrained least-square solution assumes that the following two conditions are satisfied simultaneously:

$$\sum_{k=1}^{n} f_k = 1 \text{ and } 0 \le f_k \le 1 \tag{1.2}$$

$$RMSE = \sqrt{\frac{\left(\sum_{i=1}^{m} ER_i^2\right)}{m}} \tag{1.3}$$

Estimation of end-member fraction images involves four steps, i.e. image processing, end-member selection, unmixing solution, and evaluation of fraction images. Of these steps, selecting suitable end-members is the most critical one in the development of high-quality fraction images. Two types of end-members may be applied: image end-members and reference end-members. The former are derived directly from the image itself, while the latter are derived from field measurements or the laboratory spectra of known materials (Roberts et al. 1998). Many remote sensing applications have employed image end-members, since they can be easily obtained and are capable of representing the spectra measured at the same scale as the image data itself (Roberts et al. 1998). Image end-members may be derived from the extremes of the image feature space, based on the assumption that they represent the purest pixels in the image (Boardman 1993).

1.5.1 Image Preprocessing

The study area is located at 39°46′N and 86°09′W, Marion County (the city proper of Indianapolis), Indiana, USA. According to the US Census Bureau, the county has a total area of 1044 km^2, including 1026 km^2 of land and 18 km^2 of

water. The average annual temperature is 11.7 °C with the highest temperature of 24.6 °C in July and the lowest temperature of –1.9 °C in January. Annual precipitation is evenly distributed throughout the year and average annual rainfall is 1021 mm, with the least amount of precipitation occurring in February. It is core of Indianapolis metropolitan area located in the State of Indiana. The county seat in Indianapolis was called "plain city" because of its flat topography (elevation ranges from 218 to 276 m above sea level), which provides the possibility of expansion in all directions. In recent decades, the city has been experiencing areal expansion through encroachment on agricultural land and other nonurban land due to population increases and economic growth. According to the 2010 census results, there were 904 668 people. Indianapolis has the highest concentration of major employers and manufacturing, professional, technical, and educational services in the state. With its moderate climate, rich history, excellent education, social services, arts, leisure, and recreation, Indianapolis was named as one of America's Best Places to Live and Work (Employment Review's August 1996).

Landsat TM images of 6 June 1991 (acquisition time: approximately 10 : 45 a.m.) and 3 July 1995 (approximately 10 : 28 a.m.) and a Landsat ETM+ image of 22 June 2000 (approximately 11 : 14 a.m.) were used in this study. Although the images purchased were geometrically corrected, its geometrical accuracy was determined not high enough for combining them with other high-resolution data sets. The images were therefore further rectified to a common Universal Transverse Mercator coordinate system based on 1 : 24 000 scale topographic maps and were resampled to a pixel size of 30 m for all bands using the nearest neighbor algorithm. A root-mean-square error (RMSE) of less than 0.2 pixels was obtained for all the rectifications. These Landsat images were acquired under clear sky conditions, and an improved image-based dark object subtraction model was applied to implement atmospheric corrections (Chavez 1996; Lu et al. 2002).

1.5.2 Image End-Member Development

In order to identify effectively image end-members and to achieve high-quality end-members, different image transform approaches, such as principal component analysis (PCA) and minimum noise fraction (MNF), may be applied to transform the multispectral images into a new data set (Green et al. 1988; Boardman and Kruse 1994). In this research, image end-members were selected from the feature spaces formed by the MNF components (Garcia-Haro et al. 1996; Cochrane and Souza 1998; Van der Meer and de Jong 2000; Small 2001, 2002, 2004). The MNF transform contains two steps: (i) de-correlation and rescaling of the noise in the data based on an estimated noise covariance matrix, producing transformed data in which the noise has unit variance and no band-to-band correlations, and (ii) implementation of a

standard PCA of the noise-whitened data. The result of MNF is a two-part data set, one part associated with large eigenvalues and coherent eigen-images and a complementary part associated with near-unity eigenvalues and noise-dominated images (ENVI 2000). By performing an MNF transform, noise can be separated from the data by saving only the coherent portions, thus improving spectral processing results. In this research, the MNF procedure was applied to transform the Landsat ETM+ (the 2000 image) six reflective bands into a new coordinate set. The first three MNF components accounted for the majority of the information (99%) and were used for the selection of end-members. The scatterplots between the MNF components were illustrated in Figure 1.2, showing the potential end-members. Four end-members, namely, GV, high albedo, low albedo, and soil, were finally selected. Next, a constrained

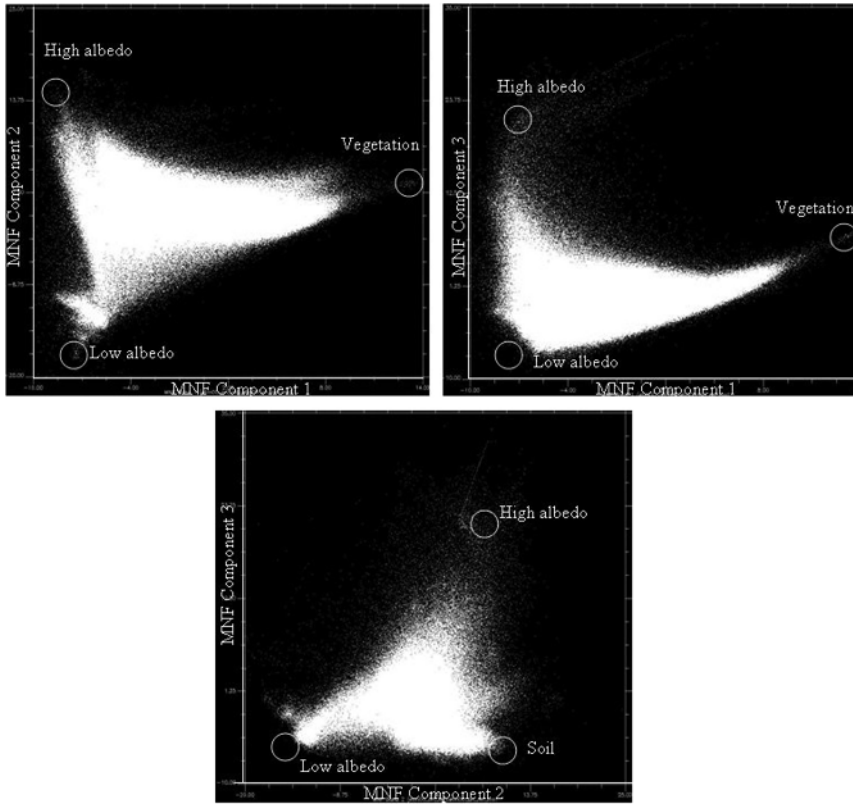

Figure 1.2 Feature spaces between the minimum noise fraction (MNF) components, illustrating potential end-members derived from a Landsat Enhanced Thematic Mapper Plus (ETM+) image. *Source:* adapted from Weng and Lu (2009). Reproduced with permission of Taylor & Francis.

least-square solution was applied to unmix the six ETM+ reflective bands into four fraction images. The same procedures were employed for derivation of fraction images from the Landsat TM 1991 and 1995 images. The first three MNF components computed from the 1991 and 1995 images also accounted for more than 99% of the scene variance, and the topologies of the triangular mixing space were consistent with that shown in Figure 1.2. Figure 1.3 shows four fraction images for the three years.

1.5.3 Extraction of Impervious Surfaces

Previous research indicated that impervious surface can be computed by adding the high- and low-albedo fractions (Wu and Murray 2003), but this method did not consider the impact of pervious surfaces on the low-albedo and high-albedo fraction images, which often resulted in overestimation of impervious surface. Our experiment with Landsat ETM+ imagery indicates that although the high-albedo fraction image related mainly to impervious surface information such as buildings and roads, it also related to other covers such as dry soils. On the other hand, the low-albedo fraction image was found to associate with water and shadows, such as water body, shadows from forest canopy and tall buildings, and moistures in crops or pastures. However, some impervious surfaces, especially dark impervious surfaces, were also linked to the low-albedo fraction image. Therefore, it is important to develop a suitable analytical procedure for removal of non-impervious information from the fraction images. In this study, we developed a procedure by using land surface temperature data to isolate non-impervious from impervious surfaces and by using soil fraction images as the thresholds to purify the high-albedo fraction images.

For the high-albedo fraction images, impervious surface was predominantly confused with dry soils. Therefore, the soil fraction images may be used to remove soils from the high-albedo fraction images. For the low-albedo fraction images, dark impervious surface was confused with water and shadows. Therefore, the critical step was to separate impervious surface from pervious pixels, including water, vegetation (forest, pasture, grass, and crops), and soils. In this study, we developed some expert rules in order to remove pervious pixels. The impervious surface image was then developed by the addition of adjusted low-albedo and high-albedo fraction images. Figure 1.4 provided a comparison of the impervious surface images before and after the adjustment. Our accuracy assessment of Landsat ETM+ image indicated that the overall RMSE of 9.22% and system error of 5.68% were obtained (Lu and Weng 2006a).

1.5.4 Image Classification

Fraction images were used for thematic land classification via a hybrid procedure that combined maximum likelihood and decision tree classifiers (Lu and

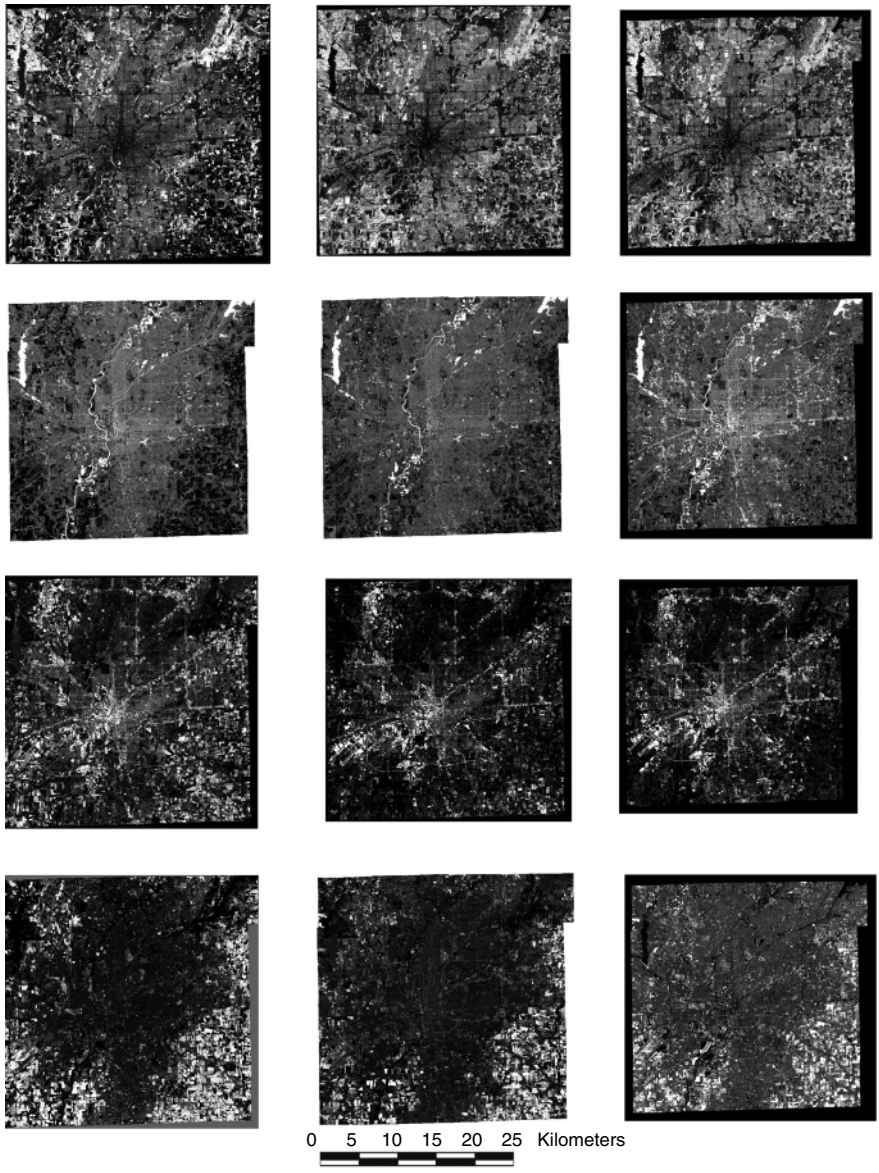

Figure 1.3 Fraction images from spectral mixture analysis of each year (First row: green vegetation; second row: low albedo; third row: high albedo; and fourth row: soil). *Source:* adapted from Weng and Lu 2006. Reproduced with permission of Taylor & Francis.

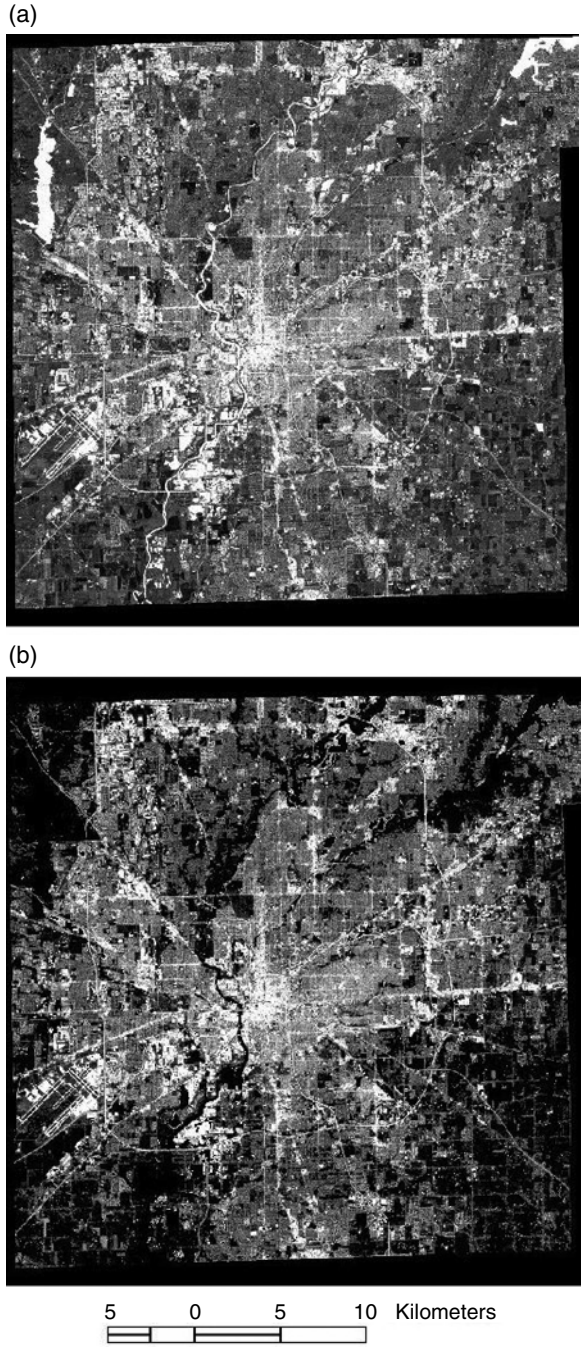

Figure 1.4 Comparison of impervious surface images developed from different methods. The image values range from 0 to 1, with lowest values in black and highest values in white. (a) Based on the direct addition of high-albedo and low-albedo fraction images. (b) Based on the addition of modified high-albedo and low-albedo fraction images, in which other covers were removed in the impervious surface image through the combined use of land surface temperature and fraction images. *Source:* adapted from Lu and Weng (2006a). Reproduced with permission of Taylor & Francis.

Weng 2004). Sample plots were identified from high-resolution aerial photographs, covering initially 10 LULC types: commercial and industrial, high-density residential, low-density residential, bare soil, crop, grass, pasture, forest, wetland, and water. On average, 10–16 sample plots for each class were selected. A window size of three by three was applied to extract the fraction value for each plot. The mean and standard deviation values were calculated for each LULC class. The characteristics of fractional composition for selected LULC types were then examined. Next, the maximum likelihood classification algorithm was applied to classify the fraction images into 10 classes, generating a classified image and a distance image. A distance threshold was selected for each class to screen out the pixels that probably do not belong to that class, which was determined by examining interactively the histogram of each class in the distance image. Pixels with a distance value greater than the threshold were assigned a class value of zero. A decision tree classifier was then applied to reclassify these pixels. The parameters required by the decision tree classifier were identified based on the mean and standard deviation of the sample plots for each class. Finally, the accuracy of the classified image was checked with a stratified random sampling method (Jensen 2005) against the reference data of 150 samples collected from large-scale aerial photographs. To simplify urban landscape analysis, 10 classes were merged into six LULC types, including (i) commercial and industrial urban land, (ii) residential land, (iii) agricultural and pasture land, (iv) grassland, (v) forest, and (vi) water (Lu and Weng 2004). Figure 1.5 shows the classified LULC maps in the three years.

The overall accuracy, producer's accuracy, and user's accuracy were calculated based on the error matrix for each classified map, as well as the KHAT statistic, kappa variance, and *Z* statistic. The overall accuracy of LULC map for 1991, 1995, and 2000 were determined to be 90, 88, and 89%, respectively. Apparently, LULC data derived from the LSMA procedure have a reasonably high accuracy and are sufficient for urban landscape analysis.

1.5.5 Urban Morphologic Analysis Based on the V-I-S Model

Three images in the first row of Figure 1.3 shows the geographic patterns of GV fractions. These images display a large dark area (low fraction values) at the center of the study area corresponding to the central business district of Indianapolis City. Bright areas of high GV values were found in the surrounding areas. Various types of crops were still at the early stage of growth or were before emergence, as indicated by medium gray to dark tone of the GV fraction images in the southeastern and southwestern parts of the city. Table 1.1 indicates that forest had the highest GV fraction values, followed by grassland. In contrast, commercial and industrial land displayed the lowest GV values. Little vegetative amount was found in water bodies, as indicated by the GV fraction values. Both residential land and pasture-agricultural land yielded a mediate

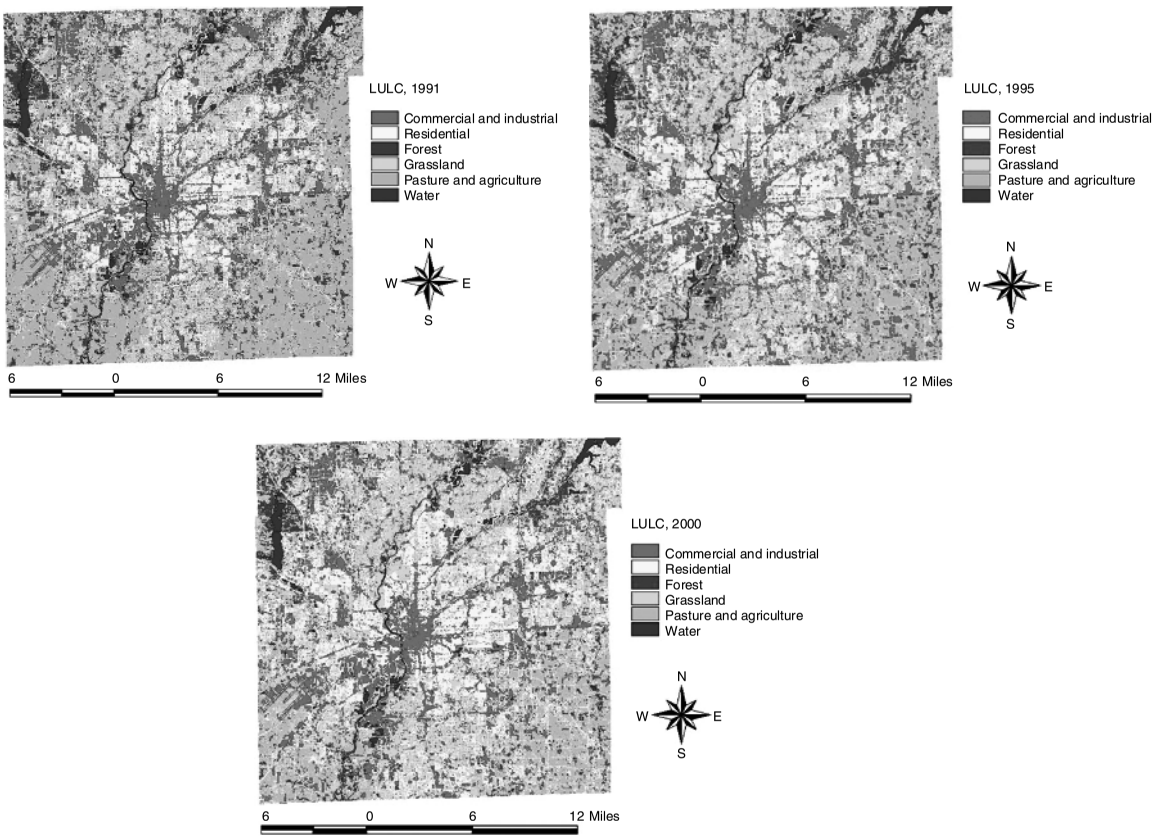

Figure 1.5 Land-use and land-cover (LULC) maps of Indianapolis in 1991, 1995, and 2000. *Source:* adapted from Weng and Lu (2006). Reproduced with permission of Taylor & Francis.

Table 1.1 V-I-S compositions of land-use and land-cover (LULC) types in Indianapolis in 1991, 1995, and 2000.

	1991 TM image			1995 TM image			2000 Enhanced Thematic Mapper Plus (ETM+) image		
Land-cover type	Mean vegetation (standard deviation)	Mean impervious surface (standard deviation)	Mean soil (standard deviation)	Mean vegetation (standard deviation)	Mean impervious surface (standard deviation)	Mean soil (standard deviation)	Mean vegetation (standard deviation)	Mean impervious surface (standard deviation)	Mean soil (standard deviation)
Commercial and industrial	0.167 (0.128)	0.709 (0.190)	0.251 (0.193)	0.127 (0.097)	0.679 (0.178)	0.273 (0.177)	0.125 (0.092)	0.681 (0.205)	0.276 (0.191)
Residential	0.314 (0.132)	0.558 (0.138)	0.198 (0.152)	0.371 (0.115)	0.508 (0.108)	0.149 (0.092)	0.298 (0.095)	0.467 (0.124)	0.247 (0.137)
Grassland	0.433 (0.176)	0.451 (0.135)	0.268 (0.208)	0.553 (0.145)	0.366 (0.096)	0.155 (0.131)	0.442 (0.099)	0.276 (0.083)	0.305 (0.119)
Agriculture and pasture	0.304 (0.213)	0.374 (0.112)	0.602 (0.285)	0.388 (0.191)	0.291 (0.091)	0.378 (0.236)	0.371 (0.168)	0.275 (0.072)	0.407 (0.222)
Forest	0.654 (0.162)	0.436 (0.128)	0.182 (0.166)	0.716 (0.085)	0.388 (0.065)	0.046 (0.052)	0.584 (0.075)	0.327 (0.074)	0.175 (0.055)
Water	0.226 (0.186)	0.730 (0.197)	0.188 (0.178)	0.176 (0.210)	0.805 (0.167)	0.094 (0.068)	0.111 (0.120)	0.891 (0.136)	0.078 (0.071)

Source: Weng and Lu (2009). Reproduced with permission of Taylor & Francis.

GV fraction value, subject to the impact of the dates of image acquired. In all the years observed, pasture-agricultural land exhibited a large standard deviation value, suggesting that pasture and agricultural land may hold various amount of vegetation.

The percentage of land covered by impervious surface may vary significantly with LULC categories and subcategories (Soil Conservation Service 1975). This study shows a substantially different estimate for each LULC type, as this study applied a spectral unmixing model to the remote sensing images, and the modeling had introduced some errors as expected. For example, a high impervious fraction value was found in water, since water related to the low-albedo fraction, and the latter were included in the computation of impervious surface. Generally speaking, an LULC type with a higher GV fraction appeared to have a lower impervious fraction. Commercial and industrial land detected very high impervious fraction values around 0.7 in all years. Residential land came after with fraction values around 0.5. Grassland, agricultural-pasture land, and forestland detected lower values of impervious surface, owing largely to their exposure to bare soil, confusion with commercial/industrial and residential land, and modeling errors.

Soil fraction values were generally low in the majority of the urban area, but high in the surroun ˙ing areas. Especially, in agricultural fields located in the southeastern and southwestern parts of the city, soil fraction images appeared very bright since various types of crops were still at the early stage of growth. Table 1.1 shows that agricultural-pasture land observed a fraction value close to 0.4 at all times. Grassland possessed medium fraction values averaging 0.25, substantially higher than the fraction values of forestland and residential land. Commercial and industrial land displayed similar fraction values as grassland, which had much to do with its confusion with dry soils in the high-albedo images. Water generally possessed a minimal impervious fraction value. Like GV fraction, soil fraction displayed the highest standard deviation values in agricultural-pasture land due to various amount of emerging vegetation.

The V-I-S composition may be examined by taking samples along transects. Figure 1.6a shows ternary plots of four transects across the geometry center of the city, sampled from the 2000 Landsat ETM+ image. Sample 1 runs from west to east, Sample 2 from north to south, Sample 3 from southwest to northeast, and Sample 4 from southeast to northwest. Errors from the spectral unmixing modeling are not included in these diagrams due to their low values clustering to near zero. Along the east–west transect, nearly all pixels sampled showed a GV fraction of less than 0.6, while soil fraction values ranged from 0.1 to 0.7. A clustering pattern was apparent, if impervious fraction values were observed in the range from 0.2 to 0.7, and GV fraction values in the range of 0.5–0.8. A more clustered pattern can be observed in the ternary diagrams based on the north–south and the southwest–northeast transects. However, the southeast–northwest transect exhibited clearly a more dispersed pattern of

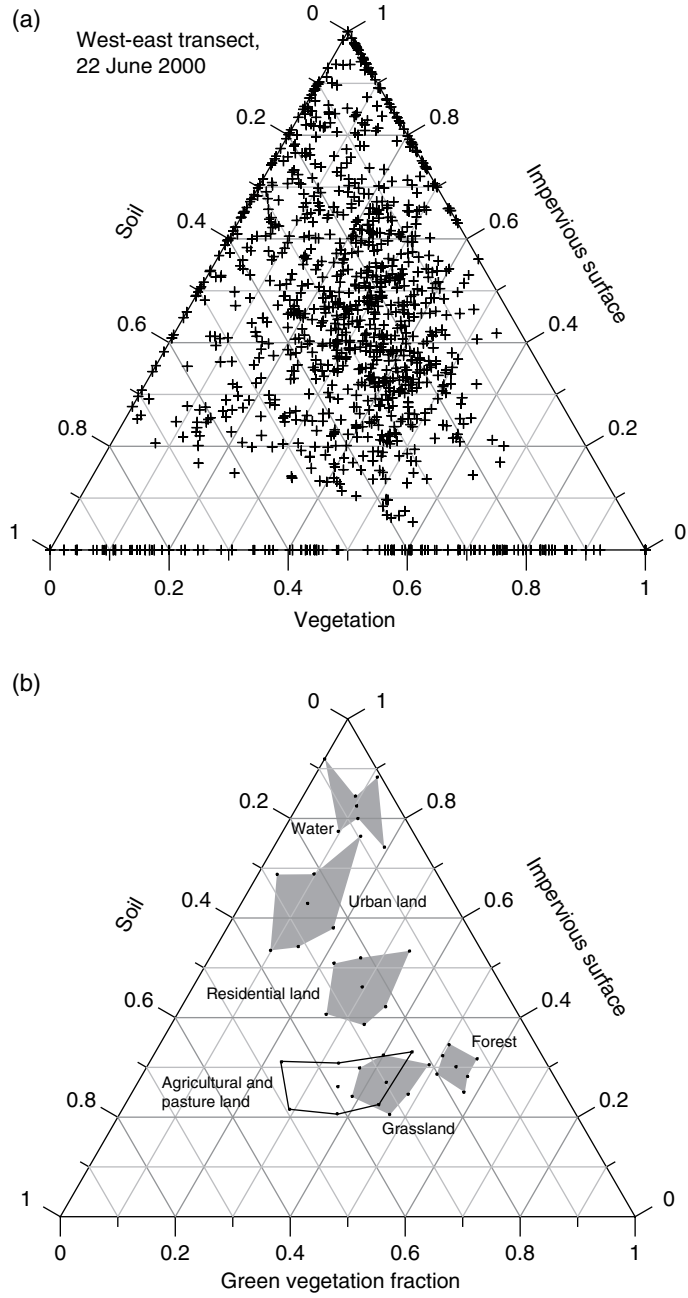

Figure 1.6 (a) Ternary plot of V-I-S composition along a sampled transect derived from Landsat ETM+ image in Indianapolis; (b) Quantitative relationships among the LULC types in respect to the V-I-S model. *Source:* adapted from Weng (2009). Reproduced with permission of the McGraw-Hill Companies, Inc.

pixel distribution, suggesting a variety of V-I-S composition types. GV along this transect yielded a fraction value from 0.3 to 1, whereas impervious fraction might have any value between 0 and 1. Soil fraction values continued to increase up to 0.8. When mean signature values of the fractions for each LULC type is plotted, quantitative relationships among the thematic LULC types in terms of the V-I-S composition can be examined. Figure 1.6b shows the V-I-S composition by LULC in 2000, with an area delineating one standard deviation from the mean fraction value.

1.5.6 Landscape Change and the V-I-S Dynamics

Table 1.2 shows the composition of LULC by year and changes occurred between two intervals. In 1991, residential use and pasture-agriculture accounted equally for 27% of the total land, while grassland shared another 20%. The combination of commercial and industrial land used 13% of the total area, and forestland had a close match, yielding another 10%. Water bodies occupied the remaining 3%, and this percentage kept unchanged from 1991 to 2000. However, LULC dynamics occurred in all other categories, as seen in the last three columns of Table 1.2. The most notable increment was observed in residential use, which grew from 27% in 1991 to 33% in 1995 reaching 38% in 2000. Associated with this change, grassland was increased from 20 to 23%. Highly developed land, mainly for commercial, industrial uses, transportation, and utilities, continued to expand. In 2000, it accounted for over 15 000 ha, or 15%, generating a 2% of increase over the nine years. These results suggest that urban land dispersal in Indianapolis was related both to population increase and to economic growth. In contrast, a pronounced decrease in pasture and agricultural land was discovered from 1991 (27%) to 1995 (20%). This decrease was also evident between 1995 and 2000, when pasture and agricultural land was further shrunk by 6581.30 ha (31.56%). Forestland in a city like Indianapolis was understandably limited in size. Our remote sensing geographic information system (GIS) analysis indicates, however, that forestland continued to disappear with a stable, marked rate. Between 1991 and 2000, forestland was reduced by 2864.81 ha (i.e. 28.75%), leveling down to approximately 7100 ha. The cross-tabulation of the 1991 and 2000 LULC maps reveals that most of the losses in pasture, agricultural, and forestland were converted to residential and other urban uses, owing to the continued process of urbanization and suburbanization. GIS overlay of the two maps further shows the spatial occurrence of urban expansion to be mostly in the edges of the city. These changes in LULC have led to changes in the composition of image fractions.

Figure 1.7 shows the pattern of changes in the V-I-S components of the LULC classes. Impervious surface, as an important urban land-cover feature, not only indicates the degree of urbanization, but also a major contributor to the environmental impacts of urbanization (Arnold and Gibbons 1996).

Table 1.2 Changes in LULC in Indianapolis, 1991–2000.

LULC type	Area, 1991 (ha)	Area, 1995 (ha)	Area, 2000 (ha)	Change, 1991–1995	Change, 1995–2000	Change, 1991–2000
Commercial and industrial	13322.10	16706.50	15489.00	3384.40 (25.40%)	−1217.50 (−7.29%)	2166.90 (16.27%)
Residential	28708.90	34123.70	40771.70	5414.80 (18.86%)	6648 (19.48%)	12062.80 (42.02%)
Grassland	21132.50	21356.60	23976.40	224.10 (1.06%)	2619.80 (12.27%)	2843.90 (13.46%)
Pasture and agriculture	28466.00	20853.80	14272.50	−7612.20 (−26.74%)	−6581.30 (−31.56%)	−14193.50 (−49.86%)
Forest	9965.58	8547.71	7100.77	−1417.87 (−14.23%)	−1446.94 (−16.93%)	−2864.81 (−28.75%)
Water	2894.21	2903.96	2903.06	9.75 (0.34%)	−0.90 (−0.03%)	8.85 (0.31%)

Source: Weng (2009). Reproduced with permission of Taylor & Francis.

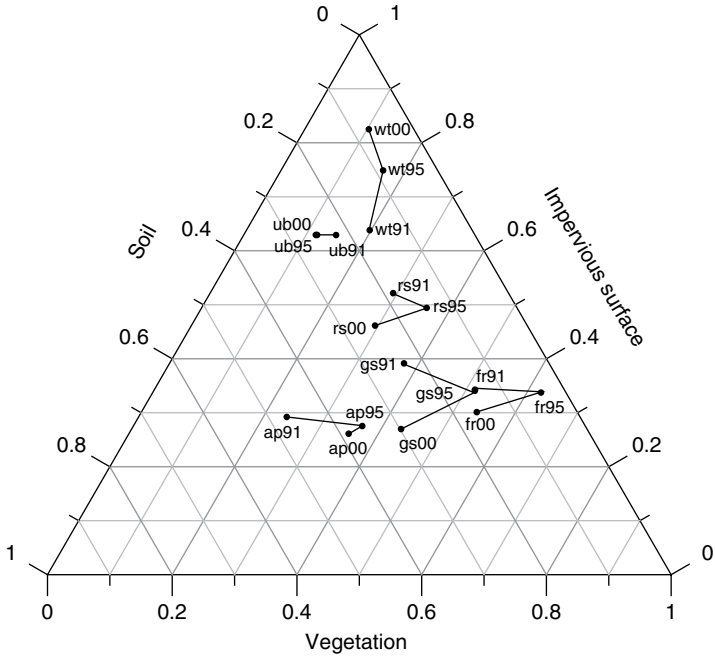

Figure 1.7 V-I-S dynamics. *Source:* Weng and Lu (2009). Reproduced with permission of Taylor & Francis.

To examine how impervious surfaces in Indianapolis had changed from 1991 to 2000, Figure 1.8 was created to show the distribution of impervious surfaces for the observed years at four categories. Result shows that the amount of pixels with values of greater than zero increased from 42 501 in 1991 to 45 804 in 1995 and further increased to 46 560 in 2000. A comparison between 1991 and 2000 indicates that this increase in the amount of pixels took place over the entire range of impervious fraction values (except for the category of 0.1–0.2). This analysis further substantiates the above findings, i.e. Indianapolis underwent an extensive urbanization process, during which impervious or impenetrable surfaces, such as rooftops, roads, parking lots, driveways, and sidewalks, were widely generated. In other words, significant amount of non-urban pixels became urbanized during the study period. Furthermore, in 1991, only 7.03% of the urbanized pixels (pixels that contain some impervious surface areas) had a value of impervious fraction greater than 0.6. In 1995 and 2000, they were 7.41 and 9.24%, respectively. This increase of pixel counts in the higher percentage categories of impervious fraction suggests that even more construction had taken place in previously urbanized pixels, i.e. there existed infill type of urban development (Wilson et al. 2003).

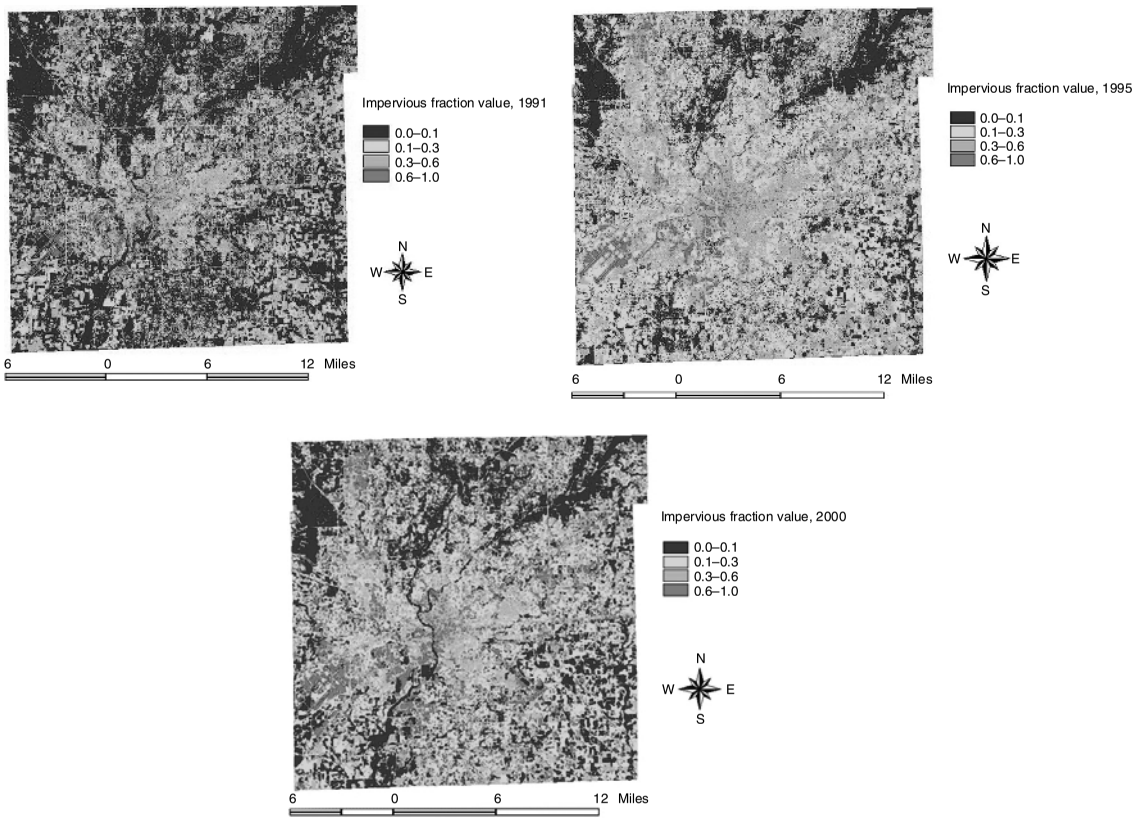

Figure 1.8 Distribution of impervious coverage by year. *Source:* adapted from Weng and Lu (2009). Reproduced with permission of Taylor & Francis.

1.6 Summary

Remote sensing of urban material, land use, and land cover has different requirements. This study intended to approach their relationship by using a continuum field model. This model was developed based on the reconciliation of the V-I-S model (Ridd 1995) and LSMA of Landsat imagery. The case study demonstrated successfully that the continuum model was effective for characterizing and quantifying the spatial and temporal changes of the landscape compositions in Indianapolis between 1991 and 2000.

The linkage between the Ridd's model and LSMA lies in the urban material. Ridd (1995) suggested that urban landscape can be decomposed into three classes of urban materials (vegetation, impervious surfaces, and soil), but did not implement the model using digital image processing algorithms. LSMA has been widely used to analyze spectrally heterogeneous urban reflectance based on "endmembers," which are recognizable surface materials that have homogenous spectral properties over the entire image. The number of endmembers that can be extracted from a satellite image is determined by the data dimensionality reflected in the image mixing space, which, in turn, is subject to the number of spectral bands available. Theoretically speaking, Landsat TM/ETM+ images, with six spectral bands (excluding the thermal infrared band), can derive as many as seven end-members. However, our study indicated that the three lower order principal components accounted for more than 99% of the image variance, implying that the mixing space was perfectly three-dimensional. The RMSE was small (less than 0.1 of mean pixel reflectance) for all three unmixings. Therefore, the end-members selected for this study (high albedo, low albedo, vegetation, and soil) were regarded proper to account for the observed radiance. When high-albedo and low-albedo end-members were used to model impervious surface, the RMSE was also found to be reasonably small for the LSMA models (less than 0.02). As such, LSMA with the four-endmember model offered a simple, robust, physically based solution to quantify the urban reflectance. Our study further indicated that although the spectral end-members were different over time because of changes in urban materials and land cover/use, the topology of the triangular mixing space was consistent. It became apparent that LSMA can provide a repetitive way to derive consistent image end-members from Landsat images. Therefore, by representing Ridd's V-I-S components as image fractions, the continuum model develop in this study provided an effective approach for quantifying urban landscape patterns as standardized component surfaces.

Existing remote sensing literature has regarded impervious surface as a type of surface material, land cover, or land use. The discrepancy in conceptual view has stimulated research into three major directions. Various sub-pixel algorithms applied largely to medium resolution but less frequently to high-resolution imagery to estimate and map impervious surfaces as a type of surface

material. Per-pixel algorithms were employed for all sorts of images at various spatial resolutions to classify impervious surfaces as a type of land cover or land use. Feature extraction methods were applied mainly to high-resolution satellite imagery, aerial photographs, and Light Detection and Ranging (LiDAR) data to extract roads and buildings, implicitly suggesting impervious surface as a special type of land use/cover. These research directions are sometime intermingled in a study, but clearly they represent different research traditions and have been approached from different perspectives. Many research endeavors have been oriented towards the spatial heterogeneity of urban landscapes, ideal spatial resolution for urban mapping, and the strengths and limitations of existing remote sensors. In contrast, less research efforts have been devoted to the spectral diversity of impervious surfaces and the spectral requirements for remote sensing of impervious surfaces. Hyperspectral imaging has been applied most extensively in the studies of vegetation and water but little to impervious surfaces. Similarly, the geometric properties (especially the 3D nature) of urban environments have been understudied. The least attention was paid to temporal resolution, change, and evolution of impervious surface over time, and temporal requirement for urban mapping. Therefore, there is a great need to address the temporal resolution requirement in urban remote sensing and how it relates to spectral resolution, spatial resolution, and the geometric characteristics of urban features and objects.

References

Adams, J.B., Sabol, D.E., Kapos, V. et al. (1995). Classification of multispectral images based on fractions of endmembers: application to land cover change in the Brazilian Amazon. *Remote Sensing of Environment* 52: 137–154.

Adams, J.B., Smith, M.O., and Johnson, P.E. (1986). Spectral mixture modeling: a new analysis of rock and soil types at the Viking Lander site. *Journal of Geophysical Research* 91: 8098–8112.

Aguiar, A.P.D., Shimabukuro, Y.E., and Mascarenhas, N.D.A. (1999). Use of synthetic bands derived from mixing models in the multispectral classification of remote sensing images. *International Journal of Remote Sensing* 20: 647–657.

Arnold, C.L. Jr. and Gibbons, C.J. (1996). Impervious surface coverage: the emergence of a key environmental indicator. *Journal of the American Planning Association* 62: 243–258.

Asner, G.P. and Lobell, D.B. (2000). A biogeophysical approach for automated SWIR unmixing of soils and vegetation. *Remote Sensing of Environment* 74: 99–112.

Bagheri, S. and Yu, T. (2008). Hyperspectral sensing for assessing nearshore water quality conditions of Hudson/Raritan estuary. *Journal of Environmental Informatics* 11 (2): 123–130.

Bauer, M.E., Loffelholz, B.C., and Wilson, B. (2007). Estimating and mapping impervious surface area by regression analysis of Landsat imagery. In: *Remote Sensing of Impervious Surfaces* (ed. Q. Weng), 3–19. Boca Raton, FL: CRC Press.

Ben-Dor, E., Levin, N., and Saaroni, H. (2001). A spectral based recognition of the urban environment using the visible and near-infrared spectral region (0.4–1.1 m) – a case study over Tel-Aviv. *International Journal of Remote Sensing* 22 (11): 2193–2218.

Benediktsson, J.A., Sveinsson, J.R., and Arnason, K. (1995). Classification and feature extraction of AVIRIS data. *IEEE Transactions on Geoscience and Remote Sensing* 33: 1194–1205.

Boardman, J.M., Kruse, F.A., and Green, R.O. (1995). Mapping target signature via partial unmixing of AVIRIS data. *Summaries of the Fifth JPL Airborne Earth Science Workshop*, JPL Publication 95-1, NASA Jet Propulsion Laboratory, Pasadena, California, pp. 23–26.

Boardman, J.W. (1993). Automated spectral unmixing of AVIRIS data using convex geometry concepts. *Summaries of the Fourth JPL Airborne Geoscience Workshop*, JPL Publication 93-26, NASA Jet Propulsion Laboratory, Pasadena, California, pp. 11–14.

Boardman, J.W. and Kruse, F.A. (1994). Automated spectral analysis: a geological example using AVIRIS data, north Grapevine Mountains, Nevada. *Proceedings, ERIM Tenth Thematic Conference on Geologic Remote Sensing*, Ann Arbor, MI, pp. 407–418.

Brun, S.E. and Band, L.E. (2000). Simulating runoff behavior in an urbanizing watershed. *Computers, Environment and Urban Systems* 24: 5–22.

Cablk, M.E. and Minor, T.B. (2003). Detecting and discriminating impervious cover with high resolution IKONOS data using principal component analysis and morphological operators. *International Journal of Remote Sensing* 24: 4627–4645.

Carlson, T.N. (2004). Analysis and prediction of surface runoff in an urbanizing watershed using satellite imagery. *Journal of the American Water Resources Association* 40 (4): 1087–1098.

Chavez, P.S. Jr. (1996). Image-based atmospheric corrections – revisited and improved. *Photogrammetric Engineering & Remote Sensing* 62: 1025–1036.

Cochrane, M.A. and Souza, C.M. Jr. (1998). Linear mixture model classification of burned forests in the eastern Amazon. *International Journal of Remote Sensing* 19: 3433–3440.

Cracknell, A.P. (1999). Twenty years of publication of the *International Journal of Remote Sensing*. *International Journal of Remote Sensing* 20: 3469–3484.

Cushnie, J.L. (1987). The interactive effect of spatial resolution and degree of internal variability within land-cover types on classification accuracies. *International Journal of Remote Sensing* 8: 15–29.

Dare, P.M. (2005). Shadow analysis in high-resolution satellite imagery of urban areas. *Photogrammetric Engineering & Remote Sensing* 71: 169–177.

ENVI (2000). *ENVI User's Guide*. Boulder, CO: Research Systems Inc.
Gamba, p. and Herold, M. (2009). *Global Mapping of Human Settlements: Experiences, Datasets, and Prospects*. Boca Raton, FL: CRC Press.
Garcia-Haro, F.J., Gilabert, M.A., and Melia, J. (1996). Linear spectral mixture modeling to estimate vegetation amount from optical spectral data. *International Journal of Remote Sensing* 17: 3373–3400.
Gillies, R.R., Box, J.B., Symanzik, J., and Rodemaker, E.J. (2003). Effects of urbanization on the aquatic fauna of the Line Creek watershed, Atlanta – a satellite perspective. *Remote Sensing of Environment* 86: 411–422.
Goetz, S.J., Wright, R.K., Smith, A.J. et al. (2003). IKONOS imagery for resource management: tree cover, impervious surfaces, and riparian buffer analyses in the mid-Atlantic region. *Remote Sensing of Environment* 88: 195–208.
Gong, p. and Howarth, P.J. (1990). The use of structure information for improving land-cover classification accuracies at the rural-urban fringe. *Photogrammetric Engineering & Remote Sensing* 56 (1): 67–73.
Gong, p. and Howarth, P.J. (1992). Frequency-based contextual classification and gray-level vector reduction for land-use identification. *Photogrammetric Engineering & Remote Sensing* 58 (4): 423–437.
Green, A.A., Berman, M., Switzer, P., and Craig, M.D. (1988). A transformation for ordering multispectral data in terms of image quality with implications for noise removal. *IEEE Transactions on Geoscience and Remote Sensing* 26: 65–74.
Heiden, U., Segl, K., Roessner, S., and Kaufmann, H. (2007). Determination of robust spectral features for identification of urban surface materials in hyperspectral remote sensing data. *Remote Sensing of Environment* 111: 537–552.
Hepner, G.F., Houshmand, B., Kulikov, I., and Bryant, N. (1998). Investigation of the integration of AVIRIS and IFSAR for urban analysis. *Photogrammetric Engineering & Remote Sensing* 64 (8): 813–820.
Herold, M. (2007). Spectral characteristics of asphalt road surfaces. In: *Remote Sensing of Impervious Surfaces* (ed. Q. Weng), 237–247. Boca Raton, FL: CRC Press.
Herold, M., Liu, X., and Clark, K.C. (2003). Spatial metrics and image texture for mapping urban land use. *Photogrammetric Engineering & Remote Sensing* 69 (9): 991–1001.
Herold, M., Schiefer, S., Hostert, P., and Roberts, D.A. (2006). Applying imaging spectrometry in urban areas. In: *Urban Remote Sensing* (eds. Q. Weng and D. Quattrochi), 137–161. Boca Raton, FL: CRC/Taylor & Francis.
Hoffbeck, J.P. and Landgrebe, D.A. (1996). Classification of remote sensing having high spectral resolution images. *Remote Sensing of Environment* 57: 119–126.
Hsieh, P.-F., Lee, L.C., and Chen, N.-Y. (2001). Effect of spatial resolution on classification errors of pure and mixed pixels in remote sensing. *IEEE Transactions on Geoscience and Remote Sensing* 39: 2657–2663.
Hu, X. and Weng, Q. (2011). Impervious surface area extraction from IKONOS imagery using an object-based fuzzy method. *Geocarto International* 26: 3–20.

Hurd, J.D. and Civco, D.L. (2004). Temporal characterization of impervious surfaces for the State of Connecticut. *ASPRS Annual Conference Proceedings*, Denver, Colorado, May 2004 (Unpaginated CD ROM).

Irons, J.R., Markham, B.L., Nelson, R.F. et al. (1985). The effects of spatial resolution on the classification of Thematic Mapper data. *International Journal of Remote Sensing* 6: 1385–1403.

Jensen, J.R. (2005). *Introductory Digital Image Processing: A Remote Sensing Perspective*, 3e. Upper Saddle River, NJ: Prentice Hall.

Jensen, J.R. and Cowen, D.C. (1999). Remote sensing of urban/suburban infrastructure and socioeconomic attributes. *Photogrammetric Engineering & Remote Sensing* 65: 611–622.

Lee, S. and Lathrop, R.G. Jr. (2005). Sub-pixel estimation of urban land cover components with linear mixture model analysis and Landsat Thematic Mapper imagery. *International Journal of Remote Sensing* 26 (22): 4885–4905.

Lillesand, T.M., Kiefer, R.W., and Chipman, J.W. (2004). *Remote Sensing and Image Interpretation*, 614. New York: Wiley.

van der Linden, S. and Hostert, p. (2009). The influence of urban structures on impervious surface maps from airborne hyperspectral data. *Remote Sensing of Environment* 113: 2298–2305.

Lu, D., Mausel, P., Brondizio, E., and Moran, E. (2002). Assessment of atmospheric correction methods for Landsat TM data applicable to Amazon basin LBA research. *International Journal of Remote Sensing* 23: 2651–2671.

Lu, D., Tian, H., Zhou, G., and Ge, H. (2008). Regional mapping of human settlements in southeastern China with multisensor remotely sensed data. *Remote Sensing of Environment* 112 (9): 3668–3679.

Lu, D. and Weng, Q. (2004). Spectral mixture analysis of the urban landscape in Indianapolis with Landsat ETM+ imagery. *Photogrammetric Engineering & Remote Sensing* 70: 1053–1062.

Lu, D. and Weng, Q. (2006a). Use of impervious surface in urban land use classification. *Remote Sensing of Environment* 102 (1–2): 146–160.

Lu, D. and Weng, Q. (2006b). Spectral mixture analysis of ASTER imagery for examining the relationship between thermal features and biophysical descriptors in Indianapolis, Indiana. *Remote Sensing of Environment* 104 (2): 157–167.

Lu, D. and Weng, Q. (2007). A survey of image classification methods and techniques for improving classification performance. *International Journal of Remote Sensing* 28 (5): 823–870.

Lu, D. and Weng, Q. (2009). Extraction of urban impervious surfaces from IKONOS imagery. *International Journal of Remote Sensing* 30 (5): 1297–1311.

Mather, P.M. (1999). Land cover classification revisited. In: *Advances in Remote Sensing and GIS* (eds. P.M. Atkinson and N.J. Tate), 7–16. New York: Wiley.

McGwire, K., Minor, T., and Fenstermaker, L. (2000). Hyperspectral mixture modeling for quantifying sparse vegetation cover in arid environments. *Remote Sensing of Environment* 72: 360–374.

Moses, W.J., Gitelson, A.A., Berdnikov, S., and Povazhnyy, V. (2009). Satellite estimation of chlorophyll-a concentration using the red and NIR bands of MERIS – The Azov Sea case study. *IEEE Geoscience and Remote Sensing Letters* 6: 845–849.

Myint, S.W. (2001). A robust texture analysis and classification approach for urban land-use and land-cover feature discrimination. *Geocarto International* 16: 27–38.

Phinn, S., Stanford, M., Scarth, p. et al. (2002). Monitoring the composition of urban environments based on the vegetation-impervious surface-soil (VIS) model by subpixel analysis techniques. *International Journal of Remote Sensing* 23: 4131–4153.

Platt, R.V. and Goetz, A.F.H. (2004). A comparison of AVIRIS and Landsat for land use classification at the urban fringe. *Photogrammetric Engineering & Remote Sensing* 70: 813–819.

Powell, R.L., Roberts, D.A., Dennison, P.E., and Hess, L.L. (2007). Sub-pixel mapping of urban land cover using multiple endmember spectral mixture analysis: Manaus, Brazil. *Remote Sensing of Environment* 106 (2): 253–267.

Pu, R., Kelly, M., Anderson, G.L., and Gong, p. (2008). Using CASI hyperspectral imagery to detect mortality and vegetation stress associated with a new hardwood forest disease. *Photogrammetric Engineering & Remote Sensing* 74 (1): 65–75.

Quattrochi, D.A. and Goodchild, M.F. (1997). *Scale in Remote Sensing and GIS*. New York City, NY: Lewis Publishers.

Rashed, T., Weeks, J.R., Roberts, D.A. et al. (2003). Measuring the physical composition of urban morphology using multiple endmember spectral mixture models. *Photogrammetric Engineering & Remote Sensing* 69: 1011–1020.

Rashed, T., Weeks, J.R., Stow, D., and Fugate, D. (2005). Measuring temporal compositions of urban morphology through spectral mixture analysis: toward a soft approach to change analysis in crowded cities. *International Journal of Remote Sensing* 26 (4): 699–718.

Ridd, M.K. (1995). Exploring a V-I-S (vegetation-impervious surface-soil) model for urban ecosystem analysis through remote sensing: comparative anatomy for cities. *International Journal of Remote Sensing* 16 (12): 2165–2185.

Roberts, D.A., Batista, G.T., Pereira, J.L.G. et al. (1998). Change identification using multitemporal spectral mixture analysis: applications in eastern Amazônia. In: *Remote Sensing Change Detection: Environmental Monitoring Methods and Applications* (eds. R.S. Lunetta and C.D. Elvidge), 137–161. Ann Arbor, MI: Ann Arbor Press.

Schmidt, K.S., Skidmore, A.K., Kloosterman, E.H. et al. (2004). Mapping coastal vegetation using an expert system and hyperspectral imagery. *Photogrammetric Engineering & Remote Sensing* 70: 703–715.

Schneider, A., Friedl, M.A., and Potere, D. (2010). Mapping global urban areas using MODIS 500-m data: New methods and datasets based on "urban ecoregions". *Remote Sensing of Environment* 114: 1733–1746.

Schueler, T.R. (1994). The importance of imperviousness. *Watershed Protection Techniques* 1: 100–111.

Shaban, M.A. and Dikshit, O. (2001). Improvement of classification in urban areas by the use of textural features: the case study of Lucknow city, Uttar Pradesh. *International Journal of Remote Sensing* 22: 565–593.

Small, C. (2001). Estimation of urban vegetation abundance by spectral mixture analysis. *International Journal of Remote Sensing* 22: 1305–1334.

Small, C. (2002). Multitemporal analysis of urban reflectance. *Remote Sensing of Environment* 81: 427–442.

Small, C. (2004). The Landsat ETM+ spectral mixing space. *Remote Sensing of Environment* 93: 1–17.

Soil Conservation Service (1975). *Urban Hydrology for Small Watersheds, USDA Soil Conservation Service Technical Release No. 55.* Washington, DC: U.S. Department of Agriculture.

Stuckens, J., Coppin, P.R., and Bauer, M.E. (2000). Integrating contextual information with per-pixel classification for improved land cover classification. *Remote Sensing of Environment* 71: 282–296.

Thenkabail, P.S., Enclona, E.A., Ashton, M.S. et al. (2004a). Hyperion, IKONOS, ALI, and ETM+ sensors in the study of African rainforests. *Remote Sensing of Environment* 90: 23–43.

Thenkabail, P.S., Enclona, E.A., Ashton, M.S., and van der Meer, B. (2004b). Accuracy assessments of hyperspectral waveband performance for vegetation analysis applications. *Remote Sensing of Environment* 91: 354–376.

Turner II, B.L., Skole, D., Sanderson, S. et al. (1995). Land-use and land-cover change: science and research plan. *International Geosphere-Biosphere Program and the Human Dimensions of Global Environmental Change Programme* (IGBP Report No. 35 and HDP Report No. 7), Stockholm and Geneva.

Van der Meer, F. and de Jong, S.M. (2000). Improving the results of spectral unmixing of Landsat Thematic Mapper imagery by enhancing the orthogonality of end-members. *International Journal of Remote Sensing* 21: 2781–2797.

Wang, F. (1990). Fuzzy supervised classification of remote sensing images. *IEEE Transactions on Geoscience and Remote Sensing* 28 (2): 194–201.

Weng, Q. (2001). Modeling urban growth effect on surface runoff with the integration of remote sensing and GIS. *Environmental Management* 28: 737–748.

Weng, Q. (2007). Remote sensing of impervious surfaces: an overview. In: *Remote Sensing of Impervious Surfaces*, xv–xxvii. Boca Raton, FL: CRC Press.

Weng, Q. (2009). Building extraction from LiDAR data. In: *Remote Sensing and GIS Integration: Theories, Methods, and Applications*, 183–208. New York: McGraw-Hill.

Weng, Q., Hu, X., and Liu, H. (2009). Estimating impervious surfaces using linear spectral mixture analysis with multi-temporal ASTER images. *International Journal of Remote Sensing* 30 (18): 4807–4830.

Weng, Q., Hu, X., and Lu, D. (2008). Extracting impervious surface from medium spatial resolution multispectral and hyperspectral imagery: a comparison. *International Journal of Remote Sensing* 29 (11): 3209–3232.

Weng, Q. and Lu, D. (2006). Sub-pixel analysis of urban landscapes. In: *Urban Remote Sensing* (eds. Q. Weng and D. Quattrochi), 71–90. Boca Raton, FL: CRC/Taylor & Francis.

Weng, Q. and Lu, D. (2009). Landscape as a continuum: an examination of the urban landscape structures and dynamics of Indianapolis city, 1991–2000. *International Journal of Remote Sensing* 30 (10): 2547–2577.

Weng, Q., Lu, D., and Schubring, J. (2004). Estimation of land surface temperature-vegetation abundance relationship for urban heat island studies. *Remote Sensing of Environment* 89: 467–483.

Wilson, E.H., Hurd, J.D., Civco, D.L. et al. (2003). Development of a geospatial model to quantify, describe and map urban growth. *Remote Sensing of Environment* 86: 275–285.

Wu, C. (2009). Quantifying high-resolution impervious surfaces using spectral mixture analysis. *International Journal of Remote Sensing* 30 (11): 2915–2932.

Wu, C. and Murray, A.T. (2003). Estimating impervious surface distribution by spectral mixture analysis. *Remote Sensing of Environment* 84: 493–505.

Wu, J.G., Jelinski, D.E., Luck, M., and Tueller, P.T. (2000). Multiscale analysis of landscape heterogeneity: scale variance and pattern metrics. *Geographic Information Sciences* 6 (1): 6–19.

Wu, J.W., Xu, J.H., and Yue, W.Z. (2005). V-I-S model for cities that are experiencing rapid urbanization and development. *Geoscience and Remote Sensing Symposium, IGARSS'05. Proceedings* 3: 1503–1506.

Yang, L., Huang, C., Homer, C.G. et al. (2003). An approach for mapping large-scale impervious surfaces: synergistic use of Landsat-7 ETM+ and high spatial resolution imagery. *Canadian Journal of Remote Sensing* 29: 230–240.